Temperature characteristics of MEMS Pressure Sensor with High Proof Pressure for Adjustable Ranges up to 10...60 kPa

M. Basov, PhD, R&D Engineer *
Dukhov Automatics Research Institute (VNIIA), Moscow 127055, Russian Federation
*Corresponding author. *E-mail address:* engineerbasovm@gmail.com (M. Basov)

ABSTRACT

Temperature characteristics are one of the key parameters determining the performance of MEMS pressure sensor under specific operating conditions. This research demonstrates a new microassembly design for differential pressure sensor with adjustable ranges of 10…60 kPa. A distinguishing feature of this microassembly is its use of stops for pressure sensor chip with sensitivity of S = 0.61 ± 0.15 mV/V/kPa. Developed pressure sensor enables to withstand proof pressure of 1.5 MPa. The proposed base geometry of the microassembly significantly reduces the impact of residual mechanical stresses (RMS) by all mechanical connections of pressure sensor chip, which is subjected to thermocycling and barocycling. It has been proven that it is possible to achieve errors in the temperature hysteresis of the zero signal (THZ) of less than 0.25%/FS in a wide temperature range from -65ºC to +85ºC, despite the requirement of top mechanical stop (as an additional source of RMS), which is only necessary to increase the overload capacity of pressure sensor.

Keywords: pressure sensor, microassembly design, high proof pressure, temperature characteristics, residual mechanical stress.

1. Introduction

Companies in the sale market of microelectromechanical systems (MEMS) pressure sensors based on the piezoresistive effect for various industrial applications are constantly focused on finding innovations in the field of design, improvement of materials and technologies, as well as in analyzing the possibilities of integration with various application platforms [1], for example, wireless implementation for Internet of Things [2], flexible pressure sensors for medicine [3] and the Industrial Internet of Things [4], ultra-high-sensitivity pressure sensors for ultra-low ranges of less than 5 kPa for a different type of applications [5-7], high-temperature SiC pressure sensors for combustion chambers in nozzles, compressors and blades for aircraft and aerospace engines [8,9], as well as combinations of pressure sensors with sensors for temperature, gas, humidity and other physical quantities [10,11]. Implementing advanced solutions requires years of validation to confirm consistent or improved performance, with multiple iterations across batches of wafers. A significant factor in development is not only the repeatability of characteristics from batch to batch, but also the stability of all parameters over time into a single batch, including errors of temperature characteristic over time [12-14].

Currently, a large number of various articles and reviews about piezoresistive pressure sensors are devoted primarily to analyzing design and technological solutions for achieving advanced mechanical performance under specific application conditions, as well as the type and nominal value of pressure. Less attention is paid to the issue of temperature influence. It is one of the most significant

factors affecting pressure sensor performance. Temperature characteristics are primarily considered by two parameters for two types of output signals:

1. The temperature coefficient of zero signal (TCZ) and temperature coefficient of sensitivity (TCS) are errors that can be compensated by application-specific integrated circuit (ASIC) [15-22] or additional circuits on the pressure-insensitive region of chip [23-25], since these errors are actually predictable in repetitions of temperature changes. Also, a temperature sensor can be created into the pressure sensor chip [26-29] or near to it in a single small-sized package [11,30] for external compensation of TCZ and TCS errors. In the present, ASIC can minimize TCZ and TCS errors, which in turn should have acceptable values of the order of no more than 0.50%/10ºC for TCZ and no more than 3.50%/10ºC for TCS.

2. Temperature hysteresis of sensitivity (THS) and, especially, temperature hysteresis of zero signal (THZ) are uncompensable errors and are quite random in nature, but within a certain error range. Therefore, the main effort is focused on finding reasons for reducing THZ and THS, which determine the final accuracy of pressure sensor.

The research analyzes issues related to the classic use of pressure sensors, which is made by monocrystalline silicon or silicon-on-isolator (SOI) structures, where piezoresistors (PRs) are not etched to buried oxide (BOX) layer. This means that the sensors operate in a temperature range of up to 90–100°C. Exceeding this temperature limit causes other factors that contribute to high errors due to a significant increase of substrate leakage current. The proposed solutions for reducing of temperature characteristic errors primarily caused by residual mechanical stresses (RMS). RMS are subject a wide range of influencing factors, including:

1. Various types of metallization with significantly higher coefficients of thermal expansion (CTE) [31-37].

2. Geometry of microassembly structure and its implementation technology for connection of pressure sensor chip [38-43].

3. Methods for connection of the microassembly structure to the sensor package [44-50].

4. The purity of diffusion and plasma processes. The presence of mobile charge in SiO_2 layers causes leakage current [51-53].

5. The doping level of impurity for PR [54-56].

6. The nominal values of RMS for compression or tension of SiO_2 and Si_3N_4 layers [57-59].

7. The resistance of the ohmic contact between the silicon and the metallization [60].

8. The RMS by the production route of pressure sensor chip itself depends on the presence of geometric asymmetry for membrane structure, process errors in lithography and diffusion [61-64].

This study, based on a large volume of experimental statistical data, examines a number of solutions for reducing temperature characteristic errors associated with both design of microassembly structure and the effects of changing the characteristics of differential pressure sensors for unjustable ranges up to 10…60 kPa after preliminary operation by thermocycling (TC) and barocycling (BC). Another distinctive feature of this microassembly designs under consideration is the presence of stops on both sides of chip to withstand a 150X proof pressure relative to the lowest differential pressure range of 10 kPa.

2. Features of pressure sensor production

2.1. Design and technology of pressure sensor chip

The main focus of this research is on the geometry of microassembly design for differential pressure sensor chip with adjustable ranges up to 10...60 kPa and the effects of preliminary operation on temperature characteristic errors. Therefore, information on the design and manufacturing technology of pressure sensor chip itself is presented as initial data for a previously developed technological route. A detailed description of all the features for the front side of pressure sensor chip (Fig. 1a) was previously presented [5, 6]. The pressure sensor chip uses Wheatstone bridge circuit with four PRs. The pressure sensor chip is manufactured from monocrystalline phosphorus-doped silicon (n-type) wafers with resistivity of ρ = 4.5 Ohm·cm, crystallographic plane (100) and thickness $W_{substrate}$ = 410 μm.

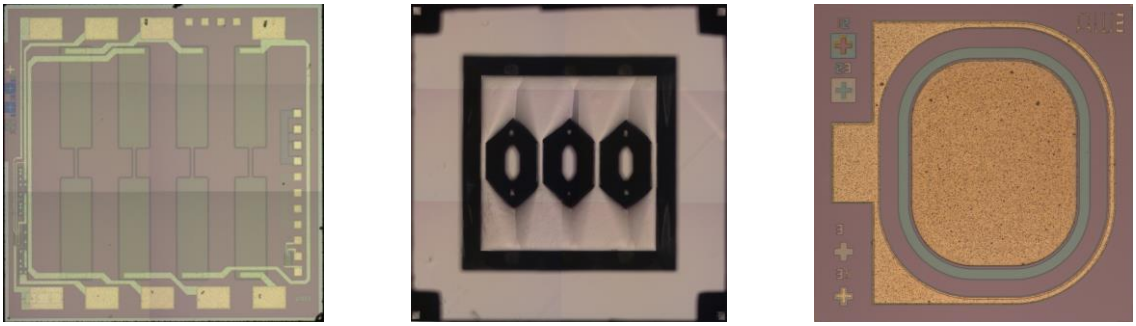

a) b) c)

Figure 1. Photo of chips for: a) pressure sensor from the front side, b) pressure sensor from the back side, c) temperature sensor.

High-boron-doped regions of the p^+-type PRs with surface concentration of $N_S = 5 \cdot 10^{19}$ cm^{-3} and piezoresistive coefficient equal to $\pi_{44} = 0.73 \cdot 10^{-9} \cdot Pa^{-1}$ is used (surface resistance R_S = 20 Ohm/□, p-n junction depth x_j = 4.0 μm) to connect low-boron-doped regions of p^--type PR with surface concentration of $N_S = 6 \cdot 10^{18}$ cm^{-3} and piezoresistive coefficient equal to $\pi_{44} = 1.26 \cdot 10^{-9} \cdot Pa^{-1}$ at room temperature (surface resistance R_S = 200 Ohm/□, p-n junction depth xj = 2.2 μm, dimensions 20x400 μm along the crystallographic direction [110]) with 0.8 μm-thick Al metallization on the non-deformable region of chip frame. The high-boron-doped p^+-type regions of PR are located on the thinned part of membrane and at least 80 μm from the membrane's etch wedge edge. This connection is crucial when designing the front side layout of pressure sensor chip to eliminate the additional influence of RMS and parasitic effects from the difference CTE between silicon and aluminum. Silicon oxide with a thickness of W_{SiO2} from 0.18 to 0.42 μm is used as an insulation layer on the front side of chip, which thickness is depending on the doping areas by lithography. The mobile charge in the insulation layer of Na^+, Cl^- and other element ions did not exceed $Q < 5 \cdot 10^{10}$ C/cm^2 after each oxidative diffusion process. A high-doped n-type region is created on the front side of chip for ohmic contact. This is necessary to apply the highest potential to the substrate, equal to the supply voltage U_{supply} = 5 V. It helps to close the p-n junction from leakage current components. Each chip is

guaranteed to achieve leakage current values I_{leak} < 10 nA at reverse bias of U_{rev} = 40 V.

The geometry structure of square membrane with thinned part and mechanical stress (SC) concentrators in the form of three rigid islands (RIs) is formed using a combination of wet anisotropic and isotropic etching only on the back side of chip (Fig. 1b), where the RIs thickness is equal to the initial wafer thickness. The geometric dimensions of chip are presented in Table 1 and, taking into account the above data about PR doping level, enable sensitivity values of at least S = 0.45 mV/V/kPa to be achieved with nonlinearity error of no more than $2K_{NL}$ = 0.20%/FS for pressure range of 60 kPa.

Table 1. Geometric dimensions of the chip and its membrane structure for differential pressure sensor with adjustable ranges up to 10…60 kPa.

Parameter	Length of the chip side	Length of the side for the thinned part of membrane	Thickness of the thinned part of membrane	The gap between RIs and the chip frame with RIs	Length of the RI edge
Dimension, μm	4000 ± 20	2200 ± 4	29 ± 2	22 ± 4	600 ± 80

In addition, developed pressure sensor also includes a separate temperature sensor chip (Fig. 1c) based on a Schottky barrier [11] with dimensions of 0.8x0.8x0.4 mm^3, which is designed both for direct measurement of temperature inside the device and for subsequent TCZ and TCS errors correction by ASIC.

2.2. Technological features of microassembly design

The choice of microassembly geometry is based on a combination of solutions to reduce the impact of RMS on temperature characteristics from all type of connections between the microassembly and pressure sensor chip inside it. This study considers the mechanism for connecting the base, chip and top mechanical stop using a glass frit [65,66], since the choice of this connection mechanism is justified by existing experience and previously achieved advantages in production (as analogy with the implementation of piezoresistive effect for pressure sensor chip). The geometry of the microassembly structure's base, as well as the methods for connecting it to the TO-8 type Kovar pakage, are based on trends identified in a comprehensive review of similar current developments [31-64,67-80]. As mentioned earlier in the Introduction, the research is presented based on statistical practical data, which collectively take into account the influence of all possible design nuances and pressure sensor manufacturing technology, as software model of complete microassembly structure often cannot account for all possible nuances of multi-stage fabrication. The main trend for the base geometry is to reduce the connection area of pressure sensor microassembly with the Kovar package, as well as to use a larger volume of the base, where mechanical decoupling from the package occurs, where the increasing the base height as much as the housing space allows. A schematic representation of the microassembly design with the main controlled dimensions is presented in Fig. 2. A monocrystalline silicon wafer with a crystallographic plane (100) and thickness of W_{base} = 3000 μm is used for the base. A Si_3N_4 layer with thickness of W_{Si3N4} = 0.15 μm is deposited on both sides by LPCVD process.

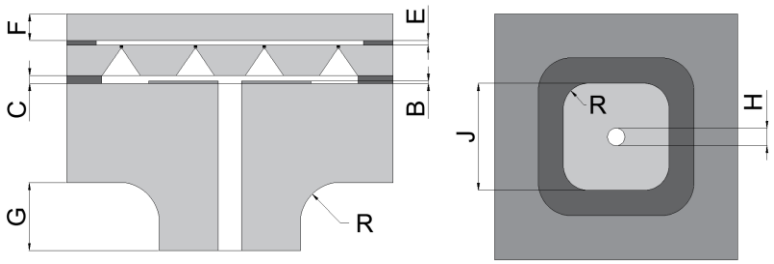

a) b)

Figure 2. Schematic representation of: a) microassembly structure (side view), b) microassembly structure (bottom view).

First, a laser process uses to form the structure of hole with diameter of H = 0.25 mm. Then the structure of base lower part is formed by laser process in form of square pedestal to depth of G = 1.00 mm and with curvature radius of R = 0.30 mm in the horizontal and vertical planes of the section. A bottom mechanical stop to depth of B = 6 μm and with area of $A_{bottom\ stop}$ = 1.90x1.90 mm^2 on the upper plane of base also formed by laser process (Fig. 3a, b). Previously, additional studies were made for this microassembly base geometry, which resulted in the determination of square pedestal side for connecting microassembly to the package (Fig. 3c). The base pedestal side should be J = 2.70 mm, considering the balance between the breakaway moment for the microassembly, bonded with organosilicon adhesive to the Kovar package, when applying proof pressure from the back of chip, and the minimum impact of RMS on temperature characteristics. The next steps of the base fabrication process involve wafer cutting and Si_3N_4 layer removing which is necessary as a barrier against the fusion of silicon dust spatter from laser process. Additionally, it is necessary to optimally eliminate potential MS concentrators into the base due to the presence of sharp corners. Therefore, in the final step, all edges of the base are isotropically etched at 50 μm to reduce the influence of MS concentrators.

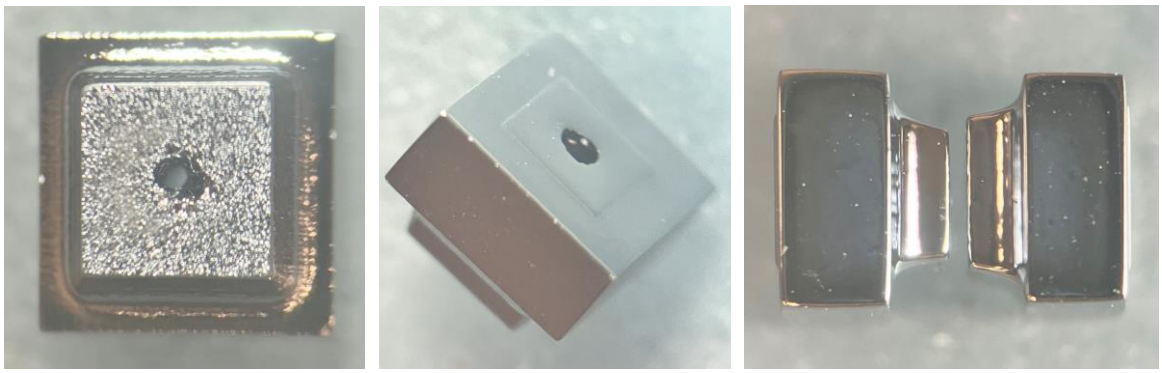

a) b) c)

Figure 3. Photo of the base for microassembly structure a) bottom view, b) angled view, c) side view with two options for the connection area of the base with package.

The top mechanical stop of microassembly is created by monocrystalline silicon wafer with crystallographic plane (100) and thickness F = 380 μm by wafer cutting with area $A_{top\ stop}$ = 2.60x4.00 mm^2. First glass frit layer is applied using a robotic installation to the upper surface of base along the

perimeter. Second glass frit layer is applied to one of the surfaces of top mechanical stop along the two smaller sides of area. The glass frit layers are subsequently vitrified at T_{vit} = 520 °C for t_{vit} = 1 hour. The final connection of all elements into the microassembly structure occurs by soldering in a vacuum $P_{vac} = 3 \cdot 10^{-4}$ Pa at temperature T_{sold} = 397 °C for t_{sold} = 20 min and torque M = 0.7 N*m (the torque acts only during the middle 10 minutes of this process). The top mechanical stop is centered relative to the pressure sensor chip during soldering to keep the contact pads open for subsequent ultrasonic welding. The spaces between the pressure sensor chip and the long sides of top mechanical stop remain open to allow pressure to be applied from the front side of chip. The resulting gaps of E = 23 ± 2 μm and C = 29 ± 3 μm (Fig. 2a) between the microassembly components differ by an amount equal to the height of bottom mechanical stop of the base B = 6 μm, since the glass frit deposited on the base is larger than on the top mechanical stop. The resulting gap dimensions are necessary for the free movement of the pressure sensor chip membrane when nominal pressure of 60 kPa is applied from either side, as well as for timely contact with the top or bottom mechanical stop before destruction by proof pressure.

Fig. 4 presents a photo of an example (one of more than 120 samples) of the developed pressure sensor and its microassembly design. An additional package cover is used, which has an hole for applying pressure from the front side of the chip.

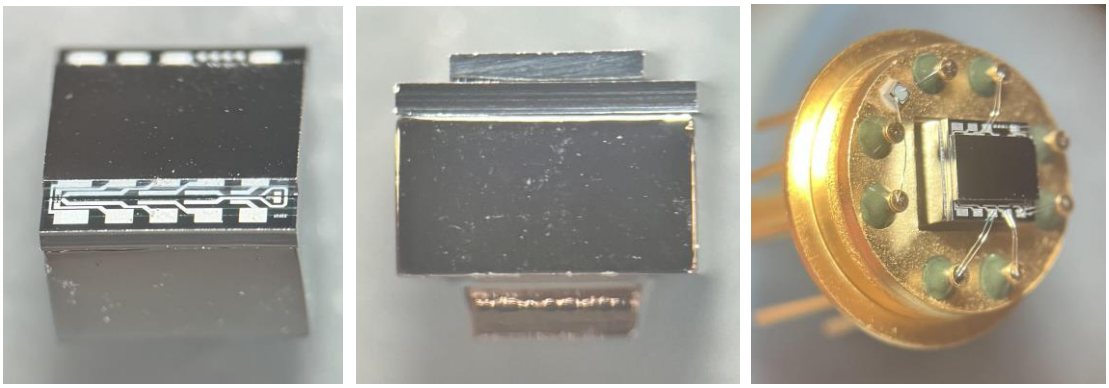

а) б) в)

Figure 4. Photo of the developed differential pressure sensor: a) microassembly design (angled view), b) microassembly design (side view), c) final view of the pressure sensor (without package cover).

The microassembly is bonded to the Kovar package by organosilicon adhesive. The process of applying and drying the organosilicon adhesive also significantly impacts by RMS on the pressure sensor chip. Therefore, the assembly should be cured for 24 hours under normal climatic conditions and then dried at T_{dry} = 250°C for t_{dry} = 1 hour after applying the adhesive to the bottom surface of microassembly and placing the microassembly inside the package without additional clamping. The condition of tightness of all connections inside the pressure sensors from helium leakage with indicators of no worse than $1 \cdot 10^{-9}$ $m^3 \cdot Pa \cdot s^{-1}$ is observed to ensure that pressure is supplied only from the front side of chip through the hole in package cover or from the back side of chip through the tube of package base.

Several factors were identified that could lead to structure failure when applying a proof

pressure of 1.5 MPa to the back of the chip. As mentioned earlier, if the bond area between the microassembly and the Kovar package is insufficient, so the organosilicon adhesive bond could fail (Fig. 5a). If the hole diameter exceeds H = 0.60 mm and the base geometry is insufficiently processed in an isotropic silicon etchant, so the base itself and the chip fail (Fig. 5b). The asymmetrical position of the top mechanical stop leads to increased stress on a single sector of the thinned part of chip membrane, resulting in failure of both elements under proof pressure (Fig. 5c).

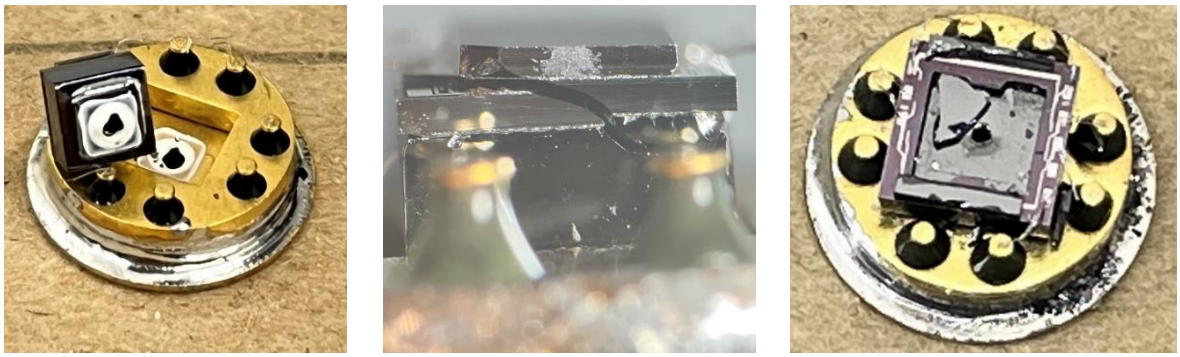

a) b) c)

Figure 5. Examples of destruction for the past versions of developed differential pressure sensor, when proof pressure attached to the back side of chip: a) separation of the microassembly from the package, b) destruction of the base and the chip into microassembly structure, c) asymmetrical connection of the top mechanical stop with the chip.

Proof pressure on either side of the pressure sensor chip could lead to premature rupture of the membrane, so as result it can be loss of sensor output signal without visual confirmation. This failure is caused by a number of factors. First, the membrane thickness, which determines its deflection when pressure is applied, can have process variability both within the 4-inch diameter wafer itself and between wafers in a batch without the use of liquid anisotropic stop-etch technology. Second, there is process variability in the height of the bottom stop of base. Third, the uniformity of glass frit application and the repeatability of vacuum soldering modes for microassembly structure can also have process variability. These factors could lead not only to burst of the chip membrane before it seats on the stop, but also to highly nonlinear output signals at nominal pressure of 60 kPa, because membrane seating is happened early. Finally, the technological solution of combination for all factors made it possible to significantly reduce technological waste to 12%.

3. Experimental research of temperature characteristics before and after TC and BC

Temperature characteristic of the developed pressure sensor is analysed inside thermal chamber Espec MC-811, which provides temperature fluctuation at a point of $\Delta T_{chamb} = \pm 0.5$ ºC and temperature gradient across the volume of $\Delta T'_{chamb} = \pm 2.0$ ºC in the range from -65 ºC to +85 ºC. As it was proved by chamber certification, the above-mentioned temperature parameters are actually significantly lower with the useful volume, which was filled with samples in special fixture by more than 50%. The temperature hysteresis of chamber at 9 points in the volume (8 edge points of the volume and 1 in the center) ranged from 0.03 to 0.15 ºC. A temperature shift of 0.15 ºC leads to an

additional component for THZ and THS of 0.004% and 0.042%, respectively, when considering the limited error indicators of the developed pressure sensors for TCZ up to 0.25%/10ºC and TCZ up to 2.80%/10ºC. Thus, temperature hysteresis has virtually no effect on TCZ, but the chamber can still makes adjustments for THS. Excess pressure is set using compressed air by WIKA Mensor CPC6050 with module up to 100 kPa and accuracy of 0.01%. The National Instruments PXI-1044 measuring system with PXI-4132 power supply (with a one-year target accuracy up to 0.025%), PXI-4071 multimeter unit (with a 90-day measurement accuracy up to 0.001%) and PXI-2527 multiplexer are used to supply power (U_{supply} = 5 V) and read the output signal.

The temperature characteristics are analyzed with the pressure sensors placed inside chamber with the midpoint for calculations at +20 ºC. Temperature characteristic measurements are divided into negative and positive temperature ranges, where THZ and THS is considered for temperature ranges of -65 to +20 ºC and +20 to +85 ºC, and TCZ and TCS is considered for temperature ranges of -30 to +20 ºC and +20 to +85 ºC. This means that output signal compensation is expected to occur in the range of -30 to +85 ºC, but the samples must guarantee low error after temperatures in the wider range of -65 to +85 ºC. All temperature characteristic calculations are based on sensitivity data when pressure is applied from the back of chip. The calculation of THZ and TCZ errors is carried out for the lowest pressure range of 10 kPa, which guarantees lower errors for intermediate ranges above (up to 60 kPa). The operating conditions for this developed pressure sensor for range up to 60 kPa are guaranteed by achieving low nonlinearity error ($2K_{NL}$ < 0.20%/FS), mechanical hysteresis (H < 0.10%/FS) and mechanical repeatability (R < 0.05%/FS). Output signal measurements are taken after 1-hour hold after the required temperature is reached in the chamber. The temperature change rate is 1.5°C/min. Tests for all temperature characteristics is conducted before and after TC and BC. The selection of TC and BC modes and methods is based on the AEC-Q100 and AEC-Q103 specifications by Automotive Electronics Council (AEC) [80]. The TC occurs in temperature range from -65°C to +130°C and consists of 50 temperature change repetitions over 150 hours. 40,000 repetitions of BC are also performed at elevated temperature of +110°C and pressure of 100 kPa applied from the back of pressure sensor chip. Table 2 presents the temperature characteristics before and after TC and BC. All parameter values are presented as "arithmetic mean ± standard deviation", where critical excesses are present, amount to less than 7% for all parameter types, and are not included in the statistical data.

Table 2. Temperature characteristic parameters of the developed pressure sensor for adjustable differential pressure range of up to 10…60 kPa.

Parameter	Temperature range, ºC	Before Tc and BC	After TC and BC
THZ, %/FS	-65…+20	0,46 ± 0,33	0,14 ± 0,09
	+20…+85	0,35 ± 0,32	0,18 ± 0,07
TCZ, %/10ºC/FS	-30…+20	0,18 ± 0,17	0,15 ± 0,12
	+20…+85	0,15 ± 0,15	0,12 ± 0,09
THS, %/FS	-65…+20	0,09 ± 0,05	0,08 ± 0,04
	+20…+85	0,05 ± 0,04	0,05 ± 0,04
TCS, %/10ºC/FS	-30…+20	2,62 ± 0,03	2,66 ± 0,04
	+20…+85	2,01 ± 0,03	2,00 ± 0,03

As discussed in the Introduction, the THS and, especially, THZ are random in nature, but within a certain error range. Therefore, the parameter results presented in Table 2 represent not only statistics between samples in a batch, but also average values from three identical measurements conducted for two temperature ranges before and after TC and BC. The obtained data clearly demonstrate the positive effect by act of TC and BC, which significantly reduces the impact of RMS for this design from all types of pressure sensor assembly operations:

1. A significant error reduction after TC and BC occurs for the most problematic parameter initially of THZ. THZ had both high values for the parameter itself and significant differences in these values between samples and between replicate measurements before TC and BC, as well as higher THZ values for the subzero temperature range. Average THZ values are reduced after TC and BC by approximately 2-3X times and the spread between samples and measurements by approximately 3-4X times.
2. The positive influence of TC and BC also affects on TCZ but not as significantly as for THZ. The average THZ values decrease by 15-20% and the variability between samples and measurements by about 30-40%..
3. Despite possible temperature hysteresis inside the chamber, THS initially has relatively small error values up to 0.15% and remains virtually unchanged after TC and BC. A similar situation is observed with relatively stable TCS values.

4. Comparative analysis of temperature characteristics with mass-produced analogues

It is necessary to consider approximately the same pressure type and range, sensitivity and proof pressure for a comparative analysis with other piezoresistive pressure sensors based on its main mechanical and temperature characteristics. The design and manufacturing technology of pressure sensor chip itself are not considered in the analysis, because there are multifactorial differences in its implementation by various companies. The output characteristics of developed pressure sensor analyzed directly with commercially available analogs [81] in Table 2, which have an analog, non-amplified output signal. The developed pressure sensor and its analogs each have their own advantages and disadvantages, which determine its specific applicability in various industrial applications. The PT2710 pressure sensor from Amphenol NovaSensors is designed for range of 17 kPa (2.5 psi), which is close to the lower limit of developed pressure sensor's range, but the analog's sensitivity is 2.3X times higher. The advantages of PT2710 include low TCZ and TCS errors, but over a narrower temperature range. The advantages of developed pressure sensor against the PT2710 include the ability to increase the proof pressure by almost 9X times. The developed microassembly design maintains same low THZ and THS errors as the analogue. TSC016KD by Honeywell has sensitivity in 2X times lower that values of the developed pressure sensor for pressure range up to 16 kPa, but its temperature characteristic errors are lower, especially for THZ. The advantages of the developed pressure sensor against TSC016KD include the ability to increase the proof pressure by almost 7.5X times and the burst pressure by 5X times. A key factor of this comparative analysis is that the developed pressure sensor is manufactured in small batches, unlike similar pressure sensors, where the annual production volume is several orders of magnitude higher.

Table 2. Comparison of temperature characteristics and proof/burst pressure for developed pressure sensor with respect to commercially available differential pressure sensors from various companies.

Company		FSUE VNIIA	Amphenol NovaSensors	NXP	Honeywell	Acuity	TE Connectivity
Modification		-	PT2710	MPX2300DT1	TSC016KD	AC3012-005-G	SMI SM9520
Pressure range ΔP	kPa	10…60	17	40	16	35	10
Sensitivity S	mV/V/kPa	0,61 ± 0,15	1,40 ± 0,35	0,04 ± 0,01	0,29 ± 0,02	0,63 ± 0,11	1,90 ± 0,60
Overall dimensions of microassembly	mm	4,0x4,0x3,8	2,0x1,6x1,0	-	-	1,8x1,6x0,4	2,1x2,1x0,6
Proof pressure ΔP_{proof}	MPa	1,50 (x25…150)	0,17 (x10)	0,86 (x22)	0,20 (x13)	0,17 (x5)	0,08 (x8)
Burst pressure ΔP_{burst}	MPa	> 2,00 (x33…200)	- -	- -	> 0,40 (x25)	> 0,52 (x15)	> 0,10 (x10)
Working test temperature range $\Delta T_{operating}$	ºC	-30…+85	0…+70	+15…+40	0…+85	+25…+70	-40…+85
Storage temperature range $\Delta T_{storage}$		-65…+85		-25…+85		-	-
TCZ	%/FS/10ºC	< 0,25	< 0,10	< 0,03	< 0,19	< 0,25	< 1,50
TCS		< 2,70	< 1,10	< 1,00	< 2,40	< 2,10	< 2,40
THZ	%/FS	< 0,25	< 0,25	-	< 0,10	-	-
THS		< 0,15					
Package		TO-8	-*	98ASB13355C	DIP/SMT/SIP	-*	-*
Presence of a temperature sensor		+	+	+	+	-	-
The presence of a compensation circuit in the housing		-	-	+	-	-	-

* - unpackaged element

5. Conclusion

This research presents the new developed microassembly design with piezoresistive pressure sensor chip for differential pressure sensor with adjustable ranges up to 10…60 kPa. A distinctive feature of the microassembly design lies in the use of stops on both sides of chip with sensitivity of S = 0.61 ± 0.15 mV/V/kPa, which withstanding the proof pressure of 1.5 MPa when applied from either side of chip. The microassembly design also use the complexly profiled base structure, which eliminates the significant impact of RMS from package and all possible mechanical connections to the

chip. The RMS reduction as temperature characteristics parameters is observed in this microassembly design after using of TC and BC, especially for THZ. The slight reduction TCZ also occurs. Changes of THS and TCS are virtually unobservable. The research demonstrates that it possible to achieve low THZ up to 0.25%/FS for the temperature range of -65…+85°C and TCZ up to 0.25%/10°C/FS for the temperature range of -30…+85°C despite the presence of the additional source for RMS in the form of the top mechanical stop, which is connected to the front side of pressure sensor chip by two glass frit layers. Achieving acceptably low temperature characteristic values without ASIC and the ability to withstand 150X-fold proof pressure for the smallest of the adjustable ranges of 10 kPa allows the development to be competitive among commercially available analogs of pressure sensor.

References

[1] Yole Group: MEMS market to grow to US$20 billion by 2028 Available online: https://www.yolegroupe.com/press-release/mems-market-to-grow-to-us20-billion-by-2028

[2] M. Barzegar, S. Blanks, S. Gharehdash, W. Timms, “Development of IOT-based low-cost MEMS pressure sensor for groundwater level monitoring”, Meas. Sci. Technol. 34 115103, DOI: https://doi.org/10.1088/1361-6501/ace78f

[3] M. S. Khan, M. O. Tariq, M. Nawaz and J. Ahmed, "MEMS Sensors for Diagnostics and Treatment in the Fight Against COVID-19 and Other Pandemics," in *IEEE Access*, vol. 9, pp. 61123-61149, 2021, DOI: https://doi.org/10.1109/ACCESS.2021.3073958

[4] Schuster, A.; Otto, A.; Rentzsch, H.; Ihlenfeldt, S. Multi-Sensory Tool Holder for Process Force Monitoring and Chatter Detection in Milling. Sensors 2024, 24, 5542, DOI: https://doi.org/10.3390/s24175542

[5] M. Basov, D. Prigodskiy, “Investigation of High Sensitivity Piezoresistive Pressure Sensors at Ultra-Low Differential Pressures,” IEEE Sensors Journal, vol. 20, no. 14, pp. 7646-7652, 2020, DOI: https://doi.org/10.1109/JSEN.2020.2980326

[6] M. Basov, D. Prigodskiy, “Development of High-Sensitivity Piezoresistive Pressure Sensors for -0.5…+0.5 kPa,” Journal of Micromechanics and Microengineering, vol. 30, no. 10, 105006, 2020, DOI: https://doi.org/10.1088/1361-6439/ab9581https://doi.org/10.1109/TIE.2017.2784341

[7] Fang, Z., Wu, X., Zhao, H. *et al.* Pt thin-film resistance thermo detectors with stable interfaces for potential integration in SiC high-temperature pressure sensors. *Microsyst Nanoeng* 10, 133 (2024), DOI: https://doi.org/10.1038/s41378-024-00746-w

[8] Meng, M., Fu, R., Xue, T. et al. Nonlinear piezoresistive effect of 4H–SiC for applications of high temperature pressure sensors. J Mater Sci 59, 18105–18119 (2024) DOI: https://doi.org/10.1007/s10853-024-10260-z

[9] Han, X., Huang, M., Wu, Z. et al. Advances in high-performance MEMS pressure sensors: design, fabrication, and packaging. Microsyst Nanoeng 9, 156 (2023), DOI: https://doi.org/10.1038/s41378-023-00620-1

[10] Basov, M. (2021). Schottky diode temperature sensor for pressure sensor. *Sensors and Actuators A: Physical*, *331*, 112930. https://doi.org/10.1016/j.sna.2021.112930

[11] S. Liu, X.H. Du, M.J. Zhu and D. Liu, Long-term Stability Enabling Technology of Silicon-

Based Piezoresistive MEMS Pressure Sensor, 2020 J. Phys.: Conf. Ser. 1520 012009 https://doi.org/10.1088/1742-6596/1520/1/012009

[12] M. Basov, "Research of MEMS Pressure Sensor Stability With PDA-NFL Circuit," in *IEEE Sensors Journal*, vol. 24, no. 21, pp. 34083-34090, 1 Nov.1, 2024, https://doi.org/10.1109/JSEN.2024.3454952

[13] M. Basov, "Research of Long-Term Stability of High-Sensitivity Piezoresistive Pressure Sensors for Ultralow Differential Pressures," in *IEEE Sensors Journal*, vol. 24, no. 22, pp. 36443-36450, 15 Nov.15, 2024, https://doi.org/10.1109/JSEN.2024.3455379

[14] Yu, Z., Zhao, Y., Li, L. et al. Realization of a micro pressure sensor with high sensitivity and overload by introducing beams and Islands. Microsyst Technol 21, 739–747 (2015) https://doi.org/10.1007/s00542-014-2234-4

[15] Brignell, J.E.; Dorey, A.P. Sensors for microprocessor-based applications. J. Phys. E Sci. Instrum. 1983, 16, 952, https://doi.org/10.1088/0022-3735/16/10/003

[16] Šaponji´c, D.; Žigic, A. Correction of a piezoresistive pressure sensor using a microcontroller. Instrum. Exp. Tech. 2001, 44, 38–44, https://doi.org/10.1023/A:1004168614028

[17] Sheng, C.C.; Hua, M.T. The research of temperature compensation technology of high-temperature pressure sensor. In Proceedings of the International Conference on Electronic and Mechanical Engineering and Information Technology, Harbin, China, 12–14 August 2011; pp. 2267–2270, https://doi.org/10.1109/EMEIT.2011.6023563

[18] Xu, D.; Liu, Y. A temperature compensation algorithm of piezoresistive pressure sensor and software implementation. In Proceedings of the IEEE International Conference on Mechatronics and Automation, Takamatsu, Japan, 4–7 August 2013; pp. 1738–1742, https://doi.org/10.1109/ICMA.2013.6618178

[19] Zhou, G.; Zhao, Y.; Guo, F.; Xu, W. A smart high accuracy silicon piezoresistive pressure sensor temperature compensation system. Sensors 2014, 14, 12174–12190, https://doi.org/10.3390/s140712174

[20] Futane, N.P.; Chowdhury, S.R.; Chowdhury, C.R.; Saha, H. ANN based CMOS ASIC design for improved temperature-drift compensation of piezoresistive micro-machined high resolution pressure sensor. Microelectron. Reliab. 2010, 50, 282–291, https://doi.org/10.1016/j.microrel.2009.09.012

[21] Futane, N.P.; Chowdhury, S.R.; Chaudhuri, C.R.; Saha, H. Analog ASIC for improved temperature drift compensation of a high sensitive porous silicon pressure sensor. Analog. Integr. Circ. Sig. Process. 2011, 67, 383–393, https://doi.org/10.1007/s10470-010-9580-7

[22] 104. Chen, G.; Sun, T.; Wang, P.; Sun, B. Design of temperature compensation system of pressure sensors. In Proceedings of the IEEE International Conference on Information Acquisition, Weihai, China, 20–23 August 2006; pp. 1042–1046, https://doi.org/10.1109/ICIA.2006.305883

[23] Yao, Z.; Liang, T.; Jia, P.; Hong, Y.; Qi, L.; Lei, C.; Zhang, B.; Xiong, J. A high-temperature piezoresistive pressure sensor with an integrated signal-conditioning circuit. Sensors 2016, 16, 913, https://doi.org/10.3390/s16060913

[24] Bao, M.H. Micro Mechanical Transducers-Pressure Sensors, Accelerometers and Gyroscopes; Elsevier B.V.: Amsterdam, The Netherlands, 2000.

[25] Wang, Q.; Ding, J.; Wang, W. Fabrication and temperature coefficient compensation technology of low cost high temperature pressure sensor. Sens. Actuators A Phys. 2005, 120, 468–473, https://doi.org/10.1016/j.sna.2005.01.036

[26] B.-N. Lee, K.-N. Kim, H.-D. Park, S.-M. Shin, “Calibration and temperature compensation of silicon pressure sensors using ion-implanted trimming resistors”, Sensors and Actuators A: Physical, Volume 72, Issue 2, 19 January 1999, Pages 148-152, DOI: https://doi.org/10.1016/S0924-4247(98)00214-3

[27] M. Mansoor, I. Haneef, S. Akhtar, M. A. Rafiq, S. Z. Ali and F. Udrea, "SOI CMOS multi-sensors MEMS chip for aerospace applications," SENSORS, 2014 IEEE, Valencia, Spain, 2014, pp. 1204-1207, https://doi.org/10.1109/ICSENS.2014.6985225

[28] Quan Wang et al., "A novel monolithically integrated pressure, accelerometer and temperature composite sensor," TRANSDUCERS 2009 - 2009 International Solid-State Sensors, Actuators and Microsystems Conference, Denver, CO, 2009, pp. 1118-1121, https://doi.org/10.1109/SENSOR.2009.5285926

[29] Z. Lan, W. Li, T. Liu, Y. Ye and X. Huang, "High-Performance Piezoresistive Pressure Sensor Based on MEMS Technology," 2025 IEEE International Conference on Electron Devices and Solid-State Circuits (EDSS), Yinchuan, China, 2025, pp. 366-368, https://doi.org/10.1109/EDSSC64492.2025.11182711

[30] Z. Guo, C. Lu, Y. Wang, D. Liu, M. Huang and X. Li, "Design and Experimental Research of a Temperature Compensation System for Silicon-on-Sapphire Pressure Sensors," in IEEE Sensors Journal, vol. 17, no. 3, pp. 709-715, 1 Feb.1, 2017, https://doi.org/10.1109/JSEN.2016.2633324

[31] J. A. Chiou and S. Chen, "Thermal hysteresis analysis of MEMS pressure sensors," in *Journal of Microelectromechanical Systems*, vol. 14, no. 4, pp. 782-787, Aug. 2005, https://doi.org/10.1109/JMEMS.2005.845460

[32] Chiang, H.-N.; Chou, T.-L.; Lin, C.-T.; Chiang, K.-N. Investigation of the hysteresis phenomenon of a silicon-based piezoresistive pressure sensor. In Proceedings of the International Microsystems, Packaging, Assembly and Circuits Technology Conference, Taipei, Taiwan, 1–3 October 2007; pp. 165–168, https://doi.org/10.1109/IMPACT.2007.4433592

[33] Eiper, E.; Resel, R.; Eisenmenger-Sittner, C.; Hafok, M.; Keckes, J. Thermally-induced stresses in thin aluminum layers grown on Silicon. Powder Di r. 2004, 19, 74–76, https://doi.org/

[34] Gardner, D.S.; Flinn, P.A. Mechanical Stress as a Function of Temperature in Aluminum Films. IEEE Trans. Electron Devices 1988, 35, 2160–2169, https://doi.org/10.1154/1.1649326

[35] Bader, S.; Kalaugher, E.M.; Arzt, E. Comparison of mechanical properties and microstructure of Al(1 wt.%Si) and Al(1 wt.%Si, 0.5 wt.%Cu) thin films. Thin Solid Films 1995, 263, 175–184, https://doi.org/10.1016/0040-6090(95)06556-3

[36] Khatibi, G.;Weiss, B.; Bernardi, J.; Schwarz, S. Microstructural Investigation of Interfacial Features in AlWire Bonds. J. Electron. Mater. 2012, 41, 3436–3446, https://doi.org/10.1007/s11664-012-2215-2

[37] M. Basov, “Pressure Sensor with New Electrical Circuit Utilizing Bipolar Junction Transistor”, IEEE Sensors, Sydney, Australia, 2021, https://doi.org/10.1109/SENSORS47087.2021.9639504

[38] M. Lishchynska, C. O'Mahony, O. Slattery, O. Wittler and H. Walter, "Evaluation of Packaging Effect on MEMS Performance: Simulation and Experimental Study," in IEEE Transactions on Advanced Packaging, vol. 30, no. 4, pp. 629-635, Nov. 2007, https://doi.org/10.1109/TADVP.2007.908026

[39] Reynolds, J.K.; Catling, D.; Blue, R.C.; Maluf, N.I.; Kenny, T. Packaging a piezoresistive pressure sensor to measure low absolute pressures over a wide sub-zero temperature range. Sens. Actuators A Phys. 2000, 83, 142–149, https://doi.org/10.1016/S0924-4247(00)00294-6

[40] Song, J.W.; Lee, J.-S.; An, J.-E.; Park, C.G. Design of a MEMS piezoresistive di erential pressure sensor with small thermal hysteresis for air data modules. Rev. Sci. Instrum. 2015, 86, 065003, https://doi.org/10.1063/1.4921862

[41] J. A. Chiou and S. Chen, “Thermal hysteresis analysis of MEMS pressure sensors,” J. Microelectromech. Syst., vol. 14, no. 4, pp. 782–787, Aug. 2005, https://doi.org/10.1109/JMEMS.2005.845460

[42] H.-N. Chiang, T.-L. Chou, C.-T. Lin, and K.-N. Chiang, “Investigation of the hysteresis phenomenon of a silicon-based piezoresistive pressure sensor,” in Proc. Int. Microsyst., Packag., Assembly Circuits Technol. (IMPACT), Oct. 2007, pp. 165–168, https://doi.org/10.1109/IMPACT.2007.4433592

[43] Chang J.-S., Lin J.-Y., Ho S.-C., Lee Y.-J. Wafer level glass frit bonding for MEMS hermetic packaging // 2010 5th International Microsystems Packaging Assembly and Circuits Technology Conference. – 2010. – P. 1-4, https://doi.org/10.1109/IMPACT.2010.5699614

[44] X. Zhang, S. Park and M. W. Judy, "Accurate Assessment of Packaging Stress Effects on MEMS Sensors by Measurement and Sensor–Package Interaction Simulations," in *Journal of Microelectromechanical Systems*, vol. 16, no. 3, pp. 639-649, June 2007, https://doi.org/10.1109/JMEMS.2007.897088

[45] R. H. Krondorfer and Y. K. Kim, "Packaging Effect on MEMS Pressure Sensor Performance," in IEEE Transactions on Components and Packaging Technologies, vol. 30, no. 2, pp. 285-293, June 2007, https://doi.org/10.1109/TCAPT.2007.898360

[46] Xu, J.; Zhao, Y.; Jiang, Z. Analysis of the packaging stresses in monolithic multi-sensor. In Proceedings of the 2nd IEEE International Conference on Nano/Micro Engineered and Molecular Systems, Bangkok, Thailand, 16–19 January 2007; pp. 241–244, https://doi.org/10.1109/NEMS.2007.352271

[47] Kim, Y.; Lee, H.; Zhang, X.; Park, S. Optimal material properties of molding compounds for MEMS package. IEEE Trans. Compon. Packag. Manuf. Technol. 2014, 4, 1589–1597, https://doi.org/10.1109/TCPMT.2014.2351574

[48] Chen, L.T.; Chang, J.S.; Hsu, C.Y.; Cheng,W.H. Fabrication and performance of MEMS-based pressure sensor packages using patterned ultra-thick photoresists. Sensors 2009, 9, 6200–6218

[49] Chen, L.-T. Packaging effect investigation of WL-CSP with a central opening: A case study on pressure sensors. Sens. Actuators A Phys. 2010, 157, 47–53, https://doi.org/10.3390/s90806200

[50] Palczynska, A.; Gromala, P.J.; Mayer, D.; Han, B.; Melz, T. In-situ investigation of EMC relaxation behavior using piezoresistive stress sensor. In Proceedings of the 16th International Conference on Thermal, Mechanical and Multi-Physics Simulation and Experiments in Microelectronics and Microsystems, Budapest, Hungary, 19–22 April 2015; pp. 1–5, https://doi.org/10.1016/j.microrel.2016.03.013

[51] Sun, Y.C.; Gao, Z.; Tian, L.Q.; Zhang, Y. Modelling of the reverse current and its effects on the thermal drift of the offset voltage for piezoresistive pressure sensors. Sens. Actuators A Phys. 2004, 116, 125–132, https://doi.org/10.1016/j.sna.2004.01.064

[52] Boukabache, A.; Pons, P.; Blasquez, G.; Dibi, Z. Characterisation and modelling of the mismatch of TCRs and their effects on the drift of the offset voltage of piezoresistive pressure sensors. Sens. Actuators A Phys. 2000, 84, 292–296, https://doi.org/10.1016/S0924-4247(00)00406-4

[53] Basov, M. (2020). High-sensitivity MEMS pressure sensor utilizing bipolar junction transistor with temperature compensation. *Sensors and Actuators A: Physical*, *303*, 111705. https://doi.org/10.1016/j.sna.2019.111705

[54] Kanda, Y. A graphical representation of the piezoresistance coefficients in silicon. IEEE Trans. Electron. Devices 1982, 29, 64–70, https://doi.org/10.1109/T-ED.1982.20659

[55] A. A. Barlian, W. -T. Park, J. R. Mallon, A. J. Rastegar and B. L. Pruitt, "Review: Semiconductor Piezoresistance for Microsystems," in Proceedings of the IEEE, vol. 97, no. 3, pp. 513-552, March 2009, https://doi.org/10.1109/JPROC.2009.2013612

[56] Basov, M. (2021). Ultra-High Sensitivity MEMS Pressure Sensor Utilizing Bipolar Junction Transistor for Pressures Ranging From −1 to 1 kPa. *IEEE Sensors Journal*, *21*(4), 4357–4364, https://doi.org/10.1109/JSEN.2020.3033813

[57] Zorman, C.A.; Roberts, R.C.; Chen, L. Additive processes for semiconductors and dielectric materials. In MEMS Materials and Processes Handbook; Ghodssi, R., Lin, P., Eds.; Springer: Boston, MA, USA, 2011; pp. 37–136, https://doi.org/10.1007/978-0-387-47318-5

[58] Basov, M. (2020). Development of high-sensitivity pressure sensor with on-chip differential transistor amplifier. *Journal of Micromechanics and Microengineering*, *30*(6), 065001. https://doi.org/10.1088/1361-6439/ab82f1

[59] Å. Sandvand, E. Halvorsen, K. E. Aasmundtveit and H. Jakobsen, "Influence of Glass-Frit Material Distribution on the Performance of Precision Piezoresistive MEMS Pressure Sensors," in IEEE Transactions on Components, Packaging and Manufacturing Technology, vol. 5, no. 11, pp. 1559-1566, Nov. 2015, https://doi.org/10.1109/TCPMT.2015.2486018

[60] Liu, G.D.; Cui, W.P.; Hu, H.; Zhang, F.S.; Zhang, Y.X.; Gao, C.C.; Hao, Y.L. High temperature pressure sensor using a thermostable electrode. In Proceedings of the 10th IEEE International Conference on Nano/Micro Engineered and Molecular Systems, Xi'an, China, 7–11 April 2015; pp. 201–204, https://doi.org/10.1109/NEMS.2015.7147410

[61] Liu, Y.; Wang, H.; Zhao, W.; Qin, H.; Fang, X., "Thermal-Performance Instability in Piezoresistive Sensors: Inducement and Improvement", Sensors 2016, 16, 1984, https://doi.org/10.3390/s16121984

[62] J. Wang and X. Li, "Single-Side Fabricated Pressure Sensors for IC-Foundry-Compatible, High-Yield, and Low-Cost Volume Production," in IEEE Electron Device Letters, vol. 32, no. 7, pp. 979-981, July 2011, https://doi.org/10.1109/LED.2011.2147272

[63] Basov, M. (2021). High sensitive, linear and thermostable pressure sensor utilizing bipolar junction transistor for 5 kPa. *Physica Scripta*, *96*(6), 065705, https://doi.org/10.1088/1402-4896/abf536

[64] S. S. Walwadkar and J. Cho, "Evaluation of die stress in MEMS packaging: Experimental and theoretical approaches," IEEE Trans. Compon. Packag. Technol., vol. 29, no. 4, pp. 735–742, Dec. 2006, https://doi.org/10.1109/TCAPT.2006.885931

[65] Knechtel R., Zellmer M., Schikowski M., Behmueller M., Buggenhout C.V., Petropoulos A. Glass Frit Wafer Bonding for Encapsulating Monolithic Integrated CMOS-MEMS Devices // ECS Transaction. – 86. – 2018. – 111, https://doi.org/10.1149/08605.0111ecst

[66] L. Li, N. Belov, M. Klitzke and J.-S. Park, "High performance piezoresistive low pressure sensors," 2016 IEEE SENSORS, Orlando, FL, USA, 2016, pp. 1-3, https://doi.org/10.1109/ICSENS.2016.7808875

[67] Waber, T., Pahl, W., Schmidt, M. et al. Temperature characterization of flip-chip packaged piezoresistive barometric pressure sensors. Microsyst Technol 20, 861–867 (2014), https://doi.org/10.1007/s00542-013-2064-9

[68] R. H. Krondorfer and Y. K. Kim, "Packaging Effect on MEMS Pressure Sensor Performance," in *IEEE Transactions on Components and Packaging Technologies*, vol. 30, no. 2, pp. 285-293, June 2007, https://doi.org/10.1109/TCAPT.2007.898360

[69] Y. Hamid, D.A. Hutt, D.C. Whalley, and R. Craddock, "Relative Contributions of Packaging Elements to the Thermal Hysteresis of a MEMS Pressure Sensor", Sensors 2020, 20(6), 1727; https://doi.org/10.3390/s20061727

[70] M. Lishchynska, C. O'Mahony, O. Slattery, O. Wittler, H. Walter, "Evaluation of Packaging Effect on MEMS Performance: Simulation and Experimental Study," in IEEE Transactions on Advanced Packaging, vol. 30, no. 4, pp. 629-635, Nov. 2007, https://doi.org/10.1109/TADVP.2007.908026

[71] Å. Sandvand, E. Halvorsen, K. E. Aasmundtveit and H. Jakobsen, "Influence of Glass-Frit Material Distribution on the Performance of Precision Piezoresistive MEMS Pressure Sensors," in IEEE Transactions on Components, Packaging and Manufacturing Technology, vol. 5, no. 11, pp. 1559-1566, Nov. 2015, https://doi.org/10.1109/TCPMT.2015.2486018

[72] S. S. Walwadkar and J. Cho, "Evaluation of die stress in MEMS packaging: Experimental and theoretical approaches," IEEE Trans. Compon. Packag. Technol., vol. 29, no. 4, pp. 735–742, Dec. 2006, https://doi.org/10.1109/TCAPT.2006.885931

[73] Albert Chiou, J., & Chen, S. (2008). Pressure nonlinearity of micromachined piezoresistive pressure sensors with thin diaphragms under high residual stresses. Sensors and Actuators A: Physical, 147(1), 332–339, https://doi.org/10.1016/j.sna.2008.03.012

[74] Å. Sandvand, E. Halvorsen, K. E. Aasmundtveit and H. Jakobsen, "Identification and Elimination of Hygro-Thermo- Mechanical Stress-Effects in a High-Precision MEMS Pressure

Sensor," in Journal of Microelectromechanical Systems, vol. 26, no. 2, pp. 415-423, April 2017, https://doi.org/10.1109/JMEMS.2017.2651162

[75] Zarnik M.S., Rocak D., Macek S. Residual stresses in a pressure-sensor package induced by adhesive material during curing: a case study // Sensors and Actuators A: Physical. – 116. – 2004. – P. 442-449, https://doi.org/10.1016/j.sna.2004.05.010

[76] Tamaki I., Tetsu O., Maasaki N., Etsutaro K., Tetsurou T., Ryuuzou A. New DPharp Series Pressure and Differential Pressure Transmitters // Yokogawa Technical Report English Edition. – 37. – 2004. – P. 9-14, https://www.yokogawa.com/library/resources/yokogawa-technical-reports/new-dpharp-ejx-series-pressure-and-differential-pressure-transmitters/

[77] Wang J., Li X. Package-friendly piezoresistive pressure sensors with on-chip integrated packaging-stress-suppressed suspension (PS3) technology // Journal of Micromechanical and Microengineering. – 23. – 2013. – 045027, https://doi.org/10.1088/0960-1317/23/4/045027

[78] Sandvand A. High-stability piezoresistive pressure sensors: PhD dissertation in Applied Micro- and Nanosystems. Kongsberg – 2017, http://hdl.handle.net/11250/2457060

[79] Å. Sandvand, E. Halvorsen and H. Jakobsen, "In Situ Observation of Metal Properties in a Piezoresistive Pressure Sensor," in *Journal of Microelectromechanical Systems*, vol. 26, no. 6, pp. 1381-1388, Dec. 2017, https://doi.org/10.1109/JMEMS.2017.2747090

[80] Automotive Electronics Council (AEC) http://www.aecouncil.com/

[81] DijiKey Corporation https://www.digikey.com/

Biographies

Mikhail Basov graduated from the National Nuclear Research University “Moscow Engineering Physics Institute” (MEPhi, Nano- and Microelectronics department, Moscow, Russia) as MSc in Electrical and Electronics Engineering. Since 2010 he currently works as R&D Engineer focused on developing MEMS piezoresistive pressure and microelectronic temperature sensors in Dukhov Authomatic Research Institute (FSUE VNIIA, Moscow, Russia). He received the Ph.D. degree from MEPhI in 2022. His PhD thesis is about creation of new pressure sensor chip with novel piezosensitive electrical circuit utilizing bipolar-junction transistor differential amplifier with negative feedback loop (PDA-NFL). He is the author of 13 articles, 22 Russian patents, and 18 conference papers. He received the award of University Technology Exposure Program by Wevolver, Mouser Electronics and ANSYS in 2022, Innovative Leader Award in the Nuclear Industry by Rosatom in 2019, and Brish Young Scientists Competition by FSUE VNIIA in 2023.

.